



# A new experimental approach and signal processing scheme for the detection and quantitation of $^{31}\text{P}$ brain neurochemicals from *in vivo* MRS studies using dual tuned ( $^1\text{H}/^{31}\text{P}$ ) head coil

Pravat K. Mandal\*, Himanshu Akolkar

Neurospectroscopy and Neuroimaging Laboratory, National Brain Research Centre, Gurgaon, India

## ARTICLE INFO

### Article history:

Received 15 July 2011

Available online 28 July 2011

### Keywords:

Human brain

$^{31}\text{P}$  MRS

High spectral resolution

Signal processing

MATLAB

## ABSTRACT

Brain  $^{31}\text{P}$ -neurometabolites play an important role in energy and membrane metabolism. Unambiguous identification and quantification of these neurochemicals in different brain regions would be a great aid in advancing the understanding of metabolic processes in the nervous system. Phosphomonoester (PME), consisting of phosphoethanolamine (PE) and phosphocholine (PC), is the “building block” for membranes, while phosphodiester (PDE), consisting of glycerophosphocholine (GPC) and glycerophosphoethanolamine (GPE) metabolites are involved in the membrane breakdown process. In the clinical setting, generating well-resolved spectra for PC, PE, GPC, and GPE could be crucial phospholipids in providing information regarding membrane metabolism. We present here a new experimental approach for generating well-resolved  $^{31}\text{P}$  spectra for PC and PE as well as for GPC, GPE, and other  $^{31}\text{P}$  metabolites. Our results (based on uni-dimensional (1D) and multi-voxel  $^{31}\text{P}$  studies) indicate that an intermediate pulse angle ( $35^\circ$ ) is best suited to obtain well-resolved PC/PE and GPC/GPE resonance peaks. Our novel signal processing scheme allows generating metabolite maps of different phospholipids include PC/PE and GPC/GPE using the ‘time-domain–frequency-domain’ method as referred to in the MATLAB programming language.

© 2011 Elsevier Inc. All rights reserved.

## 1. Introduction

Magnetic resonance spectroscopy (MRS) is a useful non-invasive imaging modality [1,2] for detecting various neurometabolites (e.g., N-acetyl aspartate (NAA), myo-inositol (ml), phosphocreatine (PCr), creatine (Cr), adenosine triphosphate (ATP), phosphomonoester (PME), phosphodiester (PDE), etc.) as well as intracellular pH [3].

Phospholipids are major constituents of both neuronal and non-neuronal cells. The phospholipids can provide a rich source of information about the functioning of neurons, since they are involved in different molecular processes ranging from energy metabolism to membrane maintenance. Phospholipids have been subject to investigation for their relevance in various brain disorders such as Alzheimer’s disease [4–8], Schizophrenia [9–11], bipolar disorder [12,13], and depression [14]. PME, consisting of phosphoethanolamine (PE) and phosphocholine (PC), primarily reflects the availability of the “membrane building block” phospholipid precursors. PDE, consisting of glycerophosphocholine (GPC) and glycerophosphoethanolamine (GPE) metabolites, indicates the level of “membrane breakdown” products. The relative amounts

of PC/PE and PME/PDE reflect the delicate balance between membrane building (anabolism) and breakdown (catabolism).

Although  $^{31}\text{P}$  MRS methodology has evolved in terms of technological development, there are still a few challenges for generating high-quality  $^{31}\text{P}$  MRS data. These intrinsic challenges are due to the low sensitivity of  $^{31}\text{P}$  nuclei, low spatial and temporal resolution, limited spectral dispersion in the absence of proton decoupling, as well as the low availability of these phospholipids. Some of these problems can be overcome by using a high field MR scanner as well as a proton decoupling scheme during  $^{31}\text{P}$  data collection. The long time requirement for performing two-dimensional (2D) and three-dimensional (3D) multi-voxel  $^{31}\text{P}$  experiments is a constraint in the clinical setting, as early availability of laboratory results may influence the course of treatment and prognostication. There is an urgent need for strategies to reduce experimental time required for multidimensional  $^{31}\text{P}$  experiments and that can be accomplished by setting optimum experimental conditions and parameters including echo time (TE), repetition time (TR), and pulse excitation angle. Transverse relaxation times of  $^{31}\text{P}$  metabolites are in the range of 20–150 ms [15] and an optimum excitation angle could have a profound role to play to effect enhanced  $^{31}\text{P}$  signal generation pertaining to high signal to noise ratio (SNR) data.

Three-dimensional  $^{31}\text{P}$  MRS studies (with proton decoupling, excitation angle  $60^\circ$ , TR = 2000 ms, TE = 2.3 ms, and NSA = 10) have revealed a significant decrease of high energy phosphates in the

\* Corresponding author. Address: National Brain Research Center, Gurgaon, India, and Adjunct Associate Professor, Radiology, Johns Hopkins Medicine, Baltimore, MD, USA.

E-mail addresses: [pravat.mandal@gmail.com](mailto:pravat.mandal@gmail.com), [pmandal4@jhui.edu](mailto:pmandal4@jhui.edu) (P.K. Mandal).

mesostriatal region of Parkinson's disease (PD) patients [16]. Larger excitation angles ranging between  $120^\circ$  and  $150^\circ$  have been applied to maximize the  $^{31}\text{P}$  signal from human brain metabolites at 3 T MRI scanner to achieve large signal gains for specific peaks of interest [17], but the peak resolution of PC/PE and GPC/GPE could not be achieved. To the best of our knowledge, there is no (*in vivo*) experimental approach to generate well-resolved PC/PE or GPC/GPE resonance peaks and subsequently quantitate them.

The focus of this study is to investigate the optimum experimental conditions for generating well resolved, high quality 1D and 2D multi-voxel  $^{31}\text{P}$  data from the human brain and develop a robust software package for  $^{31}\text{P}$  data processing using time-domain–frequency-domain (TDFD) [18] methodology in the MATLAB programming language.

## 2. Materials and methods

### 2.1. Experimental design

*In vivo*  $^{31}\text{P}$  MRS data were collected using a 3 T MRI scanner equipped with dual tuned ( $^1\text{H}/^{31}\text{P}$ ) head coil (Rapid corporation, Germany) on healthy subjects with no previous record of any neurological disorder as per the approved institutional human ethics protocol. One-dimensional  $^{31}\text{P}$  experiments were performed with the following experimental parameters (NSA = 64, TR = 650 ms, and TE = 1.2 ms, 1024 data points, SW = 4000 Hz and FOV of  $300 \times 300 \text{ mm}^2$  with 45 mm (thickness)). However, different pulse excitation angles ( $15^\circ$ ,  $35^\circ$ ,  $45^\circ$ , and  $60^\circ$ ) were applied to examine the effect of pulse excitation angle on SNR, keeping all other experimental parameters the same. The  $^1\text{H}$  decoupling was applied using WALTZ-16 [19] during acquisition of the  $^{31}\text{P}$  signal. The total time for each 1D  $^{31}\text{P}$  experiment was 1 min for each excitation angle.

Similarly, 2D multi-voxel  $^{31}\text{P}$  data were collected from the same subject with various excitation angles of  $25^\circ$ ,  $35^\circ$ , and  $45^\circ$  but the other experimental parameters (TR = 1000 ms, TE 1.4 ms, FOV of  $300 \times 300 \text{ mm}^2$  (thickness 30 mm) were kept the same.  $^{31}\text{P}$  signals

were obtained from 576 voxels (matrix of  $24 \times 24$  voxels) within field of view (FOV) of  $300 \times 300 \text{ mm}^2$  (thickness 30 mm). The  $^1\text{H}$  decoupling sequence WALTZ-16 [19] was applied during acquisition of  $^{31}\text{P}$  signals and the total experimental time for each experiment was 13 min.

### 2.2. $^{31}\text{P}$ Data processing

In our  $^{31}\text{P}$  data processing scheme, first  $^{31}\text{P}$  MRS data were processed using 3DiCSI program [20] and subsequently Fourier transformed and stored as a reference spectrum. Finally, this reference  $^{31}\text{P}$  spectrum was compared with the fitted spectrum generated through iterative procedure, using the TDFD method [18].

In the TDFD method, the MRS  $^{31}\text{P}$  signals are calculated in discrete time domain and then Fourier transformed to obtain discrete frequency domain model spectra. The algorithm can handle analytical and non-analytical line shapes. We modeled the time domain data using Voigt line shape [21,22] as shown in the following equation:

$$F(t) = \sum_{k=1}^K A(k) \times e^{i(2\pi\omega(k)\cdot n\Delta t + \phi(k))} \times e^{-l(k)\cdot n\Delta t + g(k)\cdot (n\Delta t)^2} \quad (1)$$

where  $K$  is the number of peaks and  $A(k)$ ,  $\omega(k)$ ,  $\phi(k)$ ,  $l(k)$ , and  $g(k)$  are the amplitude, chemical shift (in Hz), phase, Lorentzian and Gaussian damping factor, respectively, for  $k$ -th peak. ' $n$ ' is the sample index at which the time domain signal is sampled and ' $\Delta t$ ' is the sampling time for acquisition of this signal.

We have used prior knowledge simulating the time domain data and a total of 14  $^{31}\text{P}$  peaks (PE, PC, Pi, GPE, GPC, PCr, NAD, doublets for  $\alpha$ -ATP and  $\gamma$ -ATP, and triplet for  $\beta$ -ATP) were considered for fitting purpose. Setting the prior knowledge close to the experimental parameters (amplitude, chemical shift, linewidth, and phase) is critical for obtaining accurate quantification and convergence of the fitting, as well as for saving computational time. In our study, we have used the following prior knowledge: (1) for amplitude, maximum peak amplitude for each resonance peak was considered; (2) for chemical shift, frequency at which maximum peak

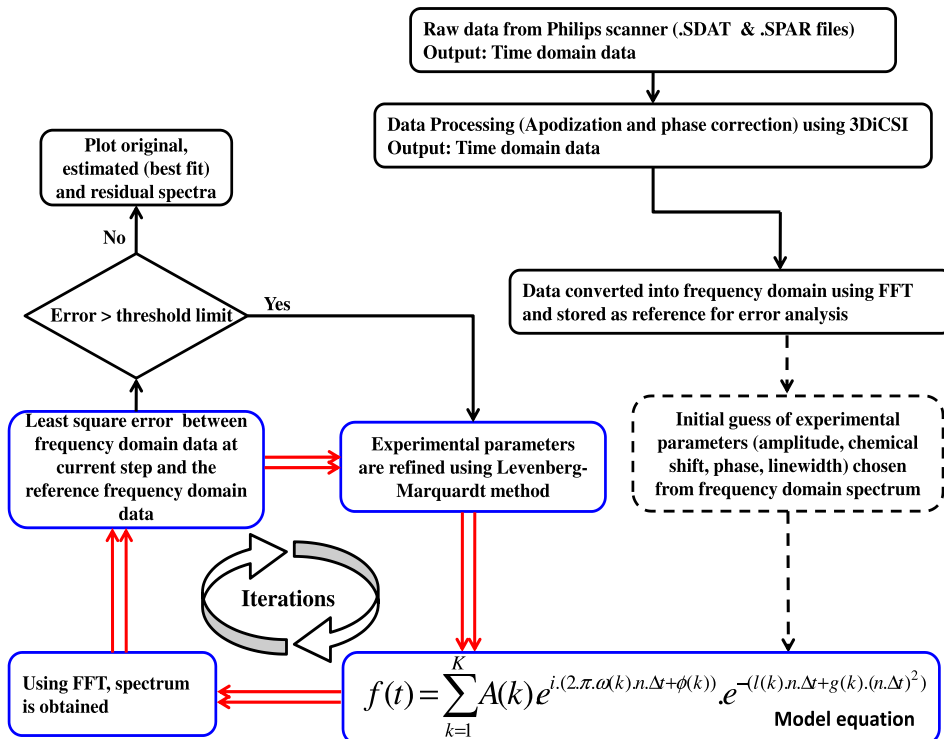
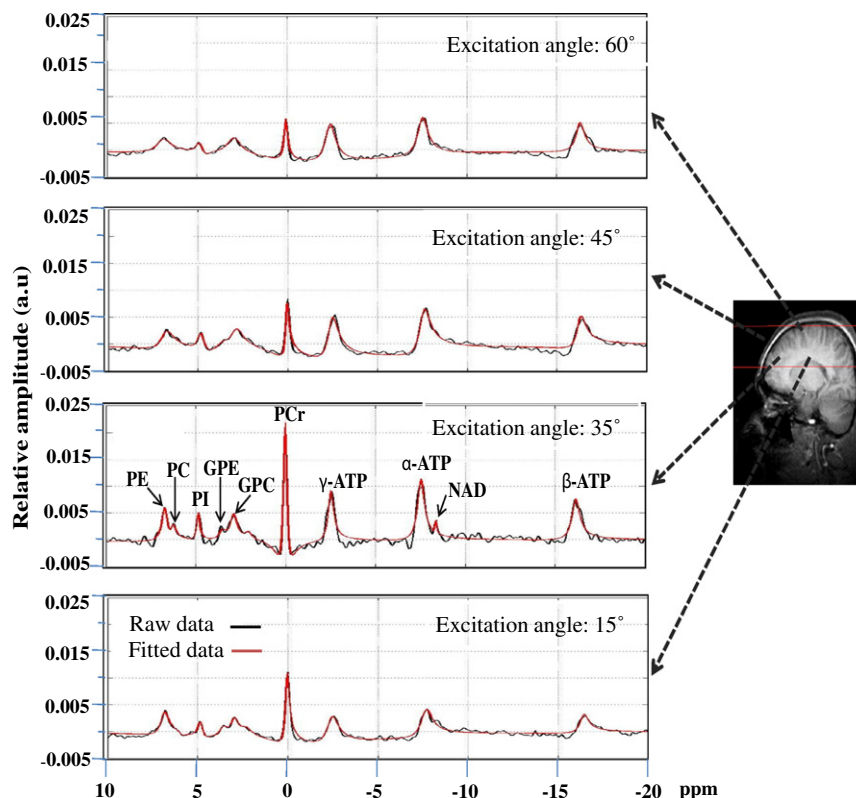


Fig. 1. Flowchart of the  $^{31}\text{P}$  data processing scheme using time-domain–frequency-domain method in MATLAB programming language.



**Fig. 2.** Stack plot of  $^{31}\text{P}$  experimental data (marked in black color) collected with various excitation angles (e.g., 25°, 35°, 45°, and 60°) and respective fitted spectra are marked in red color. The simulated data fitted extremely well with the respective experimental data indicating the robustness of our processing scheme. (For interpretation of the references to color in this figure legend, the reader is referred to the web version of this paper.)

amplitude occurs was considered; (3) for linewidth, full width at half maximum of each resonance peak was considered; (4) for phase, it is assumed to be zero for all resonance peaks obtained from the reference spectra; (5) for spectral pattern, doublets (for  $\gamma$ - and  $\alpha$ -ATP peaks with amplitude ratio 1:1) and triplets (for  $\beta$ -ATP peak with peak amplitude ratio 1:2:1) were also incorporated to simulate the time domain  $^{31}\text{P}$  data.

The iterative procedure for best experimental fitting was continued until error was lower than the predefined threshold limit in each iteration, and experimental parameters were refined using Levenberg–Marquardt nonlinear optimization (Fig. 1). After the calculated error for each of the experimental parameters (amplitude, chemical shift, linewidth, and phase) was reached within the threshold limit, the time domain data was Fourier transformed to generate a final simulated spectrum using the refined parameters obtained (amplitude, chemical shift, linewidth, and phase). Finally, the residual spectrum (difference between simulated spectrum and reference spectrum) was generated to indicate the quality of  $^{31}\text{P}$  data fitting.

### 3. Results

Our *in vivo* 1D and 2D multi-voxel  $^{31}\text{P}$  MRS studies were performed in various excitation angles. Data were processed using the processing scheme as presented in Fig. 1. Fig. 2 shows the pre-processed  $^{31}\text{P}$  spectrum and corresponding fitted 1D  $^{31}\text{P}$  spectrum performed in four excitation pulse angles (15°, 35°, 45°, and 60°). The  $^{31}\text{P}$  resonance peaks PE and PC as well as GPE and GPC are well resolved with excitation angles at 35° only and not with excitation angles 15°, 45°, and 60°. Fig. 2 also indicates that the PCr peak amplitude varies significantly with the excitation angle and PCr peak amplitude is maximum at 35° excitation angle. In order to present quantitative analysis of all  $^{31}\text{P}$  metabolites at various

excitation angles, the  $^{31}\text{P}$  peaks areas were calculated and plotted (Fig. 3). As  $^{31}\text{P}$  resonance peaks, PE and PC as well as GPC and GPE resonance were not resolved in all excitation angles, PC and PE peak areas were added together and indicated as PME; similarly, GPC and GPE peak areas were added together and leveled as PDE. The peak area for  $^{31}\text{P}$  resonance peaks (e.g., PCr, Pi, and  $\gamma$ -ATP) are much higher with 35° excitation angle (Fig. 3). [Supplementary Fig. S1](#) highlights the quality of  $^{31}\text{P}$  data fitting using our signal processing scheme. The residual peak (which is the difference between the final simulated spectrum and the reference spectrum) clearly indicates a high quality  $^{31}\text{P}$  signal processing scheme.

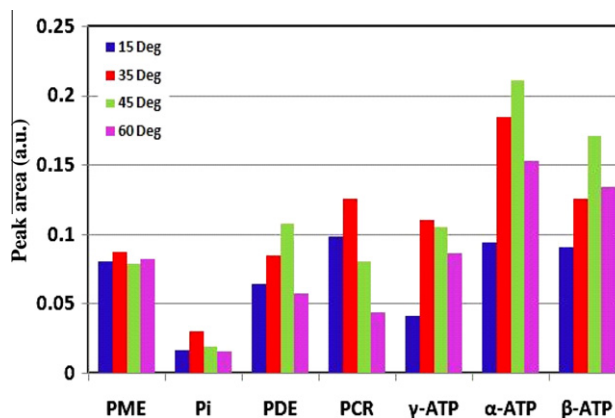


**Fig. 3.** Comparison of  $^{31}\text{P}$  peak areas of PME (PC + PE), PDE (GPC + GPE), Pi, PCr,  $\alpha$ -ATP,  $\beta$ -ATP, and  $\gamma$ -ATP in four excitation angles (15°, 35°, 45°, and 60°).  $^{31}\text{P}$  spectra of PE and PC, as well as GPC and GPE, are not well resolved at all excitation angles, except 35°, therefore PC and PE peak areas are added and represented as PME. Similarly, GPC and GPE peak areas are added together and represented as PDE. The graph shows that PME, Pi, PCR, and  $\gamma$ -ATP peak areas are higher at 35° excitation angle.

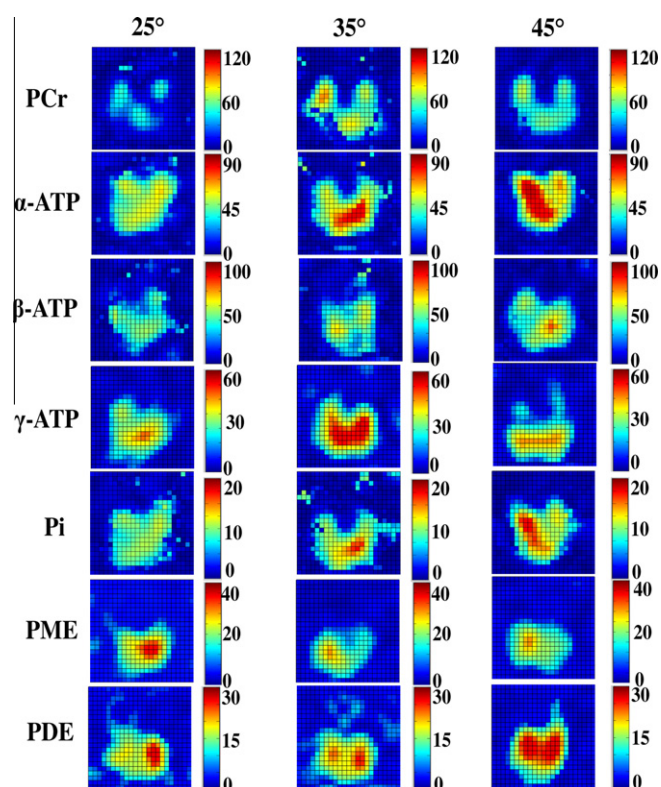


**Fig. 4.** 2D maps for metabolite areas were obtained from 2D multi-voxel  $^{31}\text{P}$  data at various excitation angles ( $25^\circ$ ,  $35^\circ$ , and  $45^\circ$ ). The 2D intensity maps show higher peak areas for PCr and  $\gamma$ -ATP at  $35^\circ$ , while PME intensities are higher in case of  $25^\circ$  excitation angle. Scale beside each of the color map indicates the gradual increment of peak area from minimum estimated area (blue) to maximum estimated peak area (red) (For interpretation of the references to color in this figure legend, the reader is referred to the web version of this paper.).

Supplementary Fig. S2 presents comparative analysis of 2D multi-voxel  $^{31}\text{P}$  MRS spectra collected using three ( $25^\circ$ ,  $35^\circ$ , and  $45^\circ$ ) pulse excitation angles. Similar to 1D  $^{31}\text{P}$  spectra (Fig. 2), in the 2D multi-voxel experiment, SNR of PCr peak is also very high at a  $35^\circ$  excitation angle compared to  $25^\circ$  and  $45^\circ$ . In order to quantitate the difference of SNR of various  $^{31}\text{P}$  resonance peaks at three excitation angles, the peak area from each voxel was calculated and is presented in Fig. 4. The relative amounts of all metabolites

(PDE, PME, Pi, PCr,  $\alpha$ -ATP,  $\beta$ -ATP, and  $\gamma$ -ATP) were assessed from the peak area using the same software package and it is found that PCr, and  $\gamma$ -ATP peak areas are higher at the  $35^\circ$  excitation angle (Fig. 4).

#### 4. Discussion

Comprehensive  $^{31}\text{P}$  MRS studies on normal subjects and Alzheimer's disease, Schizophrenia, Parkinson's disease, depression, bipolar disorder, and attention deficit hyperactivity disorder (ADHD) patients are presented in Table 1 from the existing literature. The experimental time for all these published studies is generally more than 40 min, except the MRS studies performed in 7 T MRI scanner, which is 8 min [15]. The excitation angle in various  $^{31}\text{P}$  experiments ranged from  $32^\circ$  to  $90^\circ$  (Table 1). Our *in vivo*  $^{31}\text{P}$  MRS studies have a greater potential for application in the clinical setting due to generation of high SNR  $^{31}\text{P}$  spectra with good resolution within a short period of time. A smaller excitation angle has a profound effect on resonance peaks of metabolites with shorter  $T_2$  relaxation time as well as short  $T_1$  relaxation time. Thus, a careful calibration is required to obtain an optimized excitation angle and to yield a resultant well-resolved spectrum.

The SNR of signal obtained from a metabolite depends on various experimental factors: (1) magnetic field strength  $B_0$ ; (2) optimum TR and TE; (3) optimum excitation angle. The optimal excitation angle ( $\theta$ ), known as the Ernst angle [23], for a resonance peak with relaxation time  $T_1$  and repetition time TR was given as follows:

$$\theta = \cos^{-1} (e^{-(\text{TR}/T_1)}) \quad (2)$$

Since each  $^{31}\text{P}$  metabolite has a different relaxation time, the optimum excitation pulse angle for each of them is different in a particular experimental setting. Thus, an optimum excitation angle needs to meet three criteria: (1) maximum SNR; (2) well-resolved resonance peaks; and (3) time consideration for possible application in a clinical setting. It can be noted that the calculated Ernst angle is  $34^\circ$  for PCr, within  $29$ – $42^\circ$  for PME, PDE and Pi, and  $59^\circ$  for ATP. Our experiments were performed within the span of calculated Ernst angle ( $15$ – $60^\circ$ ).

Recently, the effect of large excitation angle (LEA) was investigated to maximize SNR of  $^{31}\text{P}$  metabolites involved in bipolar disorder at 3 T MRI scanner [17]. In that LEA experimental setup, short TR and TE were used. It is interesting to note that in the LEA exper-

**Table 1**

Different  $^{31}\text{P}$  experiments in normal and diseased conditions taken from the literature. Various experimental conditions (e.g., field strength, experiment type, excitation angle field of view, brain region, and clinical status) are included. NA refers to non-availability of information.

S. No.	Field strength (Tesla)	Experiment type	Excitation angle ( $^\circ$ )	Field of view	Brain region	Clinical status	Refs.
1	1.5	2D CSI	40	$240 \times 360 \text{ mm}^2$ (30 mm slice thickness)	Prefrontal cortex; basal ganglia; temporal cortex	Normal	[25]
2	1.5	DRESS pulse	90	30 mm slice	Corpus callosum	Bipolar disorder	[13]
3	1.5	2D CSI	60	$360 \times 360 \text{ mm}^2$ (30 mm slice thickness)	Prefrontal cortex	Schizophrenia	[26]
4	4	3D CSI	32	$280 \times 280 \times 140 \text{ mm}^3$	Anterior cingulate; left thalamus	Schizophrenia	[27]
5	1.5	SV (ISIS)	NA	$28 \times 28 \times 50 \text{ mm}^3$	Left prefrontal cortex	AD	[4]
6	1.5	SV	NA	$15\text{--}20 \text{ cm}^3$	Dorsal prefrontal cortex	AD	[6]
7	1.5	SV	90	50 slice thickness	Orbito-frontal Occipital lobe	Normal subjects	[28]
8	1.5	SV	90	$30 \times 30 \times 50 \text{ mm}^3$	Basal ganglia	Depression	[29]
9	1.5	SV	90	50 mm slice thickness	Orbito- frontal occipital lobe	Depression	[30]
10	1.5	2D CSI	NA	$240 \times 360 \text{ mm}^2$ (30 mm slice thickness)	Prefrontal cortex; basal ganglia;	ADHD	[31]
11	1.5	SV	40–60	–	Visual cortex	PD	[32]
12	3	3D CSI	60	$300 \times 300 \times 200 \text{ mm}^3$	NA	PD	[16]
13	1.5	DRESS	NA	25 mm slice thickness	Occipital lobe	MSA; PD;	[33]
14	4	3D CSI	37	$240 \times 240 \times 240 \text{ mm}^3$	Whole brain	Normal	[34]

iments, the observed maximum amplitude of peaks at various excitation angles (e.g., PCr at 140°, PC at 120°, Pi at 120°, ATP at 120°, etc.) were reported [17]. It is worthwhile to mention that PC and PE as well as GPC and GPE peaks were not resolved in the LEA experiments [17]. In our study, <sup>31</sup>P experiments with excitation angle of 35°, it was not only the PC and PE peaks and the GPC and GPE peaks that were well resolved, but the amplitude of the four peaks (PME, PCr, Pi, and  $\gamma$ -ATP) were also higher, compared to any other excitation angles (Supplementary Figs. S1 and 3). A similar trend is also observed in 2D multi-voxel <sup>31</sup>P data (Fig. 4), where the peak area of PCr, and  $\gamma$ -ATP are much higher in the same voxel of the same subject at 35° compared to other excitation pulses (45° or 25°).

#### 4.1. Iterative procedure using TDFD methodology

We have demonstrated by using optimum experimental conditions (e.g., excitation angle 35°) that all <sup>31</sup>P resonance peaks are well resolved. The <sup>31</sup>P data processing scheme for multi-voxel studies using TDFD is robust, fast, and user-friendly. Other researchers have reported <sup>31</sup>P data processing (ATP level and pH) using SAGE/IDL software, but the reported <sup>31</sup>P data quality (poor SNR) acted as a hindrance to obtain any quantitative measure of these metabolites [24]. In this context, our MATLAB based software package is extremely useful in generating intensity maps from high quality <sup>31</sup>P data generated through new experimental approach.

#### Acknowledgments

Dr. Pravat K. Mandal thanks the Department of Biotechnology, Government of India for funding this research. The discussion with Dr. Jeffery Stanley (Wayne State University, Michigan) and Dr. Subulakshmy Natarajan (MBBS, Ph.D.) is appreciated.

#### Appendix A. Supplementary data

Supplementary data associated with this article can be found, in the online version, at doi:10.1016/j.bbrc.2011.07.088.

#### References

- [1] P.K. Mandal, In vivo proton magnetic resonance spectroscopic signal processing for the absolute quantitation of brain metabolites, *European Journal of Radiology* (2011).
- [2] P.K. Mandal, Magnetic resonance spectroscopy (MRS) and its application in Alzheimer's disease, *Concepts in Magnetic Resonance* 23 (2007) 40–65.
- [3] N. Patel, D.M. Forton, G.A. Coutts, H.C. Thomas, S.D. Taylor-Robinson, Intracellular pH measurements of the whole head and the basal ganglia in chronic liver disease: a phosphorus-31 MR spectroscopy study, *Metabolic Brain Disease* 15 (2000) 223–240.
- [4] O.V. Forlenza, P. Wacker, P.V. Nunes, J. Yacubian, C.C. Castro, M.C. Otaduy, W.F. Gattaz, Reduced phospholipid breakdown in Alzheimer's brains: a <sup>31</sup>P spectroscopy study, *Psychopharmacology* 180 (2005) 359–365.
- [5] R.G. Gonzalez, A.R. Guimaraes, G.J. Moore, A. Crawley, L.A. Cupples, J.H. Growdon, Quantitative in vivo <sup>31</sup>P magnetic resonance spectroscopy of Alzheimer disease, *Alzheimer Disease and Associated Disorders* 10 (1996) 46–52.
- [6] J.W. Pettegrew, K. Panchalingam, W.E. Klunk, R.J. McClure, L.R. Muenz, Alterations of cerebral metabolism in probable Alzheimer's disease: a preliminary study, *Neurobiology of Aging* 15 (1994) 117–132.
- [7] R. Longo, A. Giorgini, S. Magnaldi, L. Pascasio, C. Ricci, Alzheimer's disease histologically proven studied by MRI and MRS: two cases, *Magnetic Resonance Imaging* 11 (1993) 1209–1215.
- [8] Y. Mashima, H. Yamada, K. Koyama, [Dementia and human in vivo <sup>31</sup>P-MRS], *Nippon rinsho, Japanese Journal of Clinical Medicine* 49 (1991) 1656–1659.
- [9] J.E. Jensen, J. Miller, P.C. Williamson, R.W. Neufeld, R.S. Menon, A. Malla, R. Manchanda, B. Schaefer, M. Densmore, D.J. Drost, Grey and white matter differences in brain energy metabolism in first episode schizophrenia: <sup>31</sup>P-MRS chemical shift imaging at 4 Tesla, *Psychiatry Research* 146 (2006) 127–135.
- [10] R.A. Komoroski, J.M. Pearce, R.E. Mrak, <sup>31</sup>P NMR spectroscopy of phospholipid metabolites in postmortem schizophrenic brain, *Magnetic Resonance in Medicine* 59 (2008) 469–474.
- [11] A.D. Hinsberger, P.C. Williamson, T.J. Carr, J.A. Stanley, D.J. Drost, M. Densmore, G.C. MacFabe, D.G. Montemurro, Magnetic resonance imaging volumetric and phosphorus 31 magnetic resonance spectroscopy measurements in schizophrenia, *Journal of Psychiatry and Neuroscience* 22 (1997) 111–117.
- [12] H. Hamakawa, J. Murashita, N. Yamada, T. Inubushi, N. Kato, T. Kato, Reduced intracellular pH in the basal ganglia and whole brain measured by <sup>31</sup>P-MRS in bipolar disorder, *Psychiatry and Clinical Neurosciences* 58 (2004) 82–88.
- [13] T. Kato, T. Shioiri, S. Takahashi, T. Inubushi, Measurement of brain phosphoinositide metabolism in bipolar patients using in vivo <sup>31</sup>P-MRS, *Journal of Affective Disorders* 22 (1991) 185–190.
- [14] D.V. Iosifescu, P.E. Renshaw, <sup>31</sup>P-magnetic resonance spectroscopy and thyroid hormones in major depressive disorder: toward a bioenergetic mechanism in depression?, *Harvard Review of Psychiatry* 11 (2003) 51–63.
- [15] H. Lei, X.H. Zhu, X.L. Zhang, K. Ugurbil, W. Chen, In vivo <sup>31</sup>P magnetic resonance spectroscopy of human brain at 7 T: an initial experience, *Magnetic Resonance in Medicine* 49 (2003) 199–205.
- [16] E. Hattingen, J. Magerkurth, U. Pilatus, A. Mozer, C. Seifried, H. Steinmetz, F. Zanella, R. Hilker, Phosphorus and proton magnetic resonance spectroscopy demonstrates mitochondrial dysfunction in early and advanced Parkinson's disease, *Brain* 132 (2009) 3285–3297.
- [17] R.A. Blenman, J.D. Port, J.P. Felmler, Selective maximization of (31)P MR spectroscopic signals of in vivo human brain metabolites at 3 T, *Journal of Magnetic Resonance Imaging* 25 (2007) 628–634.
- [18] J. Slotboom, C. Boesch, R. Kreis, Versatile frequency domain fitting using time domain models and prior knowledge, *Magnetic Resonance in Medicine* 39 (1998) 899–911.
- [19] A.J. Shaka, J. Keeler, T. Frenkiel, A. Freeman, An improved sequence for broadband decoupling: WALTZ-16, *Journal of Magnetic Resonance* 52 (1983) 335–338.
- [20] Q. Zhao, P. Patriotis, F. Arias-Mendoza, R. Stoyanova, T.R. Brown, 3D interactive chemical shift imaging: a comprehensive software program for data analysis and quantification, in: 48th ENC Experimental Nuclear Magnetic Resonance Conference, 2007.
- [21] I. Marshall, S.D. Bruce, J. Higinbotham, A. MacLulich, J.M. Wardlaw, K.J. Ferguson, J. Seckl, Choice of spectroscopic lineshape model affects metabolite peak areas and area ratios, *Magnetic Resonance in Medicine* 44 (2000) 646–649.
- [22] L. Vanhamme, T. Sundin, P.V. Hecke, S.V. Huffel, MR spectroscopy quantitation: a review of time-domain methods, *NMR in Biomedicine* 14 (2001) 233–246.
- [23] R.R. Ernst, W.A. Anderson, Application of Fourier transform spectroscopy to magnetic resonance, *Review of Scientific Instruments* 37 (1966) 93–102.
- [24] P. Wu, W. Liu, Y. Chen, H. Wang, Z. Shen, K. Brügge, D.J. Mikulis, Preliminary study of mapping brain ATP and brain pH using multivoxel <sup>31</sup>P MR spectroscopy ICBME, in: Proceedings, 2009.
- [25] G. Goldstein, K. Panchalingam, R.J. McClure, J.A. Stanley, V.D. Calhoun, G.D. Pearlson, J.W. Pettegrew, Molecular neurodevelopment: an in vivo <sup>31</sup>P-<sup>1</sup>H MRSI study, *Journal of the International Neuropsychological Society* 15 (2009) 671–683.
- [26] M.S. Keshavan, J.A. Stanley, D.M. Montrose, N.J. Minshew, J.W. Pettegrew, Prefrontal membrane phospholipid metabolism of child and adolescent offspring at risk for schizophrenia or schizoaffective disorder: an in vivo <sup>31</sup>P MRS study, *Molecular Psychiatry* 8 (2003) 316–323. 251.
- [27] J. Theberge, Y. Al-Semaan, J.E. Jensen, P.C. Williamson, R.W. Neufeld, R.S. Menon, B. Schaefer, M. Densmore, D.J. Drost, Comparative study of proton and phosphorus magnetic resonance spectroscopy in schizophrenia at 4 Tesla, *Psychiatry Research* 132 (2004) 33–39.
- [28] I.K. Lyoo, S.W. Kong, S.M. Sung, F. Hirashima, A. Parow, J. Hennen, B.M. Cohen, P.F. Renshaw, Multinuclear magnetic resonance spectroscopy of high-energy phosphate metabolites in human brain following oral supplementation of creatine-mono-hydrate, *Psychiatry Research* 123 (2003) 87–100.
- [29] C.M. Moore, J.D. Christensen, B. Lafer, M. Fava, P.F. Renshaw, Lower levels of nucleoside triphosphate in the basal ganglia of depressed subjects: a phosphorus-31 magnetic resonance spectroscopy study, *American Journal of Psychiatry* 154 (1997) 116–118.
- [30] M.M. Silveri, A.M. Parow, R.A. Villafuerte, K.E. Damico, J. Goren, A.L. Stoll, B.M. Cohen, P.F. Renshaw, S-Adenosyl-L-methionine: effects on brain bioenergetic status and transverse relaxation time in healthy subjects, *Biological Psychiatry* 54 (2003) 833–839.
- [31] J.A. Stanley, H. Kipp, E. Greisenegger, F.P. MacMaster, K. Panchalingam, J.W. Pettegrew, M.S. Keshavan, O.G. Bukstein, Regionally specific alterations in membrane phospholipids in children with ADHD: an in vivo <sup>31</sup>P spectroscopy study, *Psychiatry Research* 148 (2006) 217–221.
- [32] M. Rango, C. Bonifati, N. Bresolin, Parkinson's disease and brain mitochondrial dysfunction: a functional phosphorus magnetic resonance spectroscopy study, *Journal of Cerebral Blood Flow and Metabolism* 26 (2006) 283–290.
- [33] B. Barbiroli, P. Martinelli, A. Patuelli, R. Lodi, S. Iotti, P. Cortelli, P. Montagna, Phosphorus magnetic resonance spectroscopy in multiple system atrophy and Parkinson's disease, *Movement Disorders* 14 (1999) 430–435.
- [34] H.P. Hetherington, D.D. Spencer, J.T. Vaughan, J.W. Pan, Quantitative (31)P spectroscopic imaging of human brain at 4 Tesla: assessment of gray and white matter differences of phosphocreatine and ATP, *Magnetic Resonance in Medicine* 45 (2001) 46–52.